

# Collective Synchronization Induced by Epidemic Dynamics on Complex Networks with Communities

Gang Yan<sup>1</sup>, Zhong-Qian Fu<sup>1,\*</sup>, Jie Ren<sup>2</sup>, and Wen-Xu Wang<sup>2</sup>

<sup>1</sup>*Department of Electronic Science and Technology,*

*University of Science and Technology of China, Hefei, Anhui, 230026, P.R.China*

<sup>2</sup>*Nonlinear Science Center and Department of Modern Physics,*

*University of Science and Technology of China, Hefei, Anhui, 230026, P.R.China*

(Dated: October 17, 2018)

Much recent empirical evidence shows that *community structure* is ubiquitous in the real-world networks. In this Letter, we propose a growth model to create scale-free networks with the tunable strength (noted by  $Q$ ) of community structure and investigate the influence of community strength upon the collective synchronization induced by SIRS epidemiological process. Global and local synchronizability of the system is studied by means of an order parameter and the relevant finite-size scaling analysis is provided. The numerical results show that, a phase transition occurs at  $Q_c \simeq 0.835$  from global synchronization to desynchronization and the local synchronization is weakened in a range of intermediately large  $Q$ . Moreover, we study the impact of mean degree  $\langle k \rangle$  upon synchronization on scale-free networks.

PACS numbers: 89.75.-k, 89.75.Fb, 89.75.Hc

*I. Introduction.*—The study of networked systems, including technological, social and biological networks of various kinds, has attracted much attention in physics community [1, 2, 3, 4]. How the properties of networks, such as the lengths of shortest paths between vertices, degree distribution, clustering coefficient, degree-degree correlation and so on, affect dynamical processes taking place upon the networks [5, 6, 7, 8, 9, 10], has been one of the most important subjects of the body of work. Recently, it has been determined that many real-world networks show *community structure* [11, 12], i.e., groups of vertices that have a high density of edges within them, while a lower density of edges between groups. However, there's few work about the influences of various degree of community structure upon dynamics.

In this paper, we intend to fill this gap by investigating synchronization behavior induced by the SIRS epidemiological dynamics [13, 14] on the scale-free networks with various strength (noted by  $Q$ ) of community structure. In Ref. [15], the authors have studied the SIRS on small-world networks and found that when  $p$ , which characterizes the degree of disorder of the network, reach an intermediately large value  $p_c$ , synchronization of the system emerges. Comparatively, we focus on global and local (inside each community) dynamics, and discover that no synchronization comes forth when the network possesses strong enough community structure, i.e. the communities are connected by few edges among them. Moreover, the vertices inside each community behave weaker synchronization when  $Q$  is in a range of intermediately large values.

*II. Network Model.*—To generally characterize the community structure of scale-free networks, we propose a

growth model to create a network with a tunable parameter denoting the strength of community structure. Inspired by two ingredients of Barabasi-Albert model (BA for short), i.e., growth and preferential attachment [16], the rules of our model are as follows: Starting with  $c$  communities, noted by  $U_1, U_2, \dots, U_{c-1}, U_c$ , and each community with a small number ( $m_0$ ) of vertices. At every time step, we add into each community a new vertex with  $m (< m_0)$  edges that link the new vertex to  $n$  different vertices in this community and  $m - n$  different vertices in other  $c - 1$  communities already existed in the system. The initial  $m_0 \times c$  vertices link to each other to keep the connectivity of the network. The values of  $m$  and  $n$  are not necessary integers (take  $m$  for example: the fractional part of  $m$  denotes the probability to link  $m' + 1$  different vertices, where  $m'$  is the integral part of  $m$ ). When adding a new vertex into community  $U_l$ , firstly choose  $n$  different vertices in community  $U_l$  according to “preferential attachment”, which means the probability  $\prod$  that the new vertex will connect to vertex  $i$  ( $i \in U_l$ ) depends on the degree  $k_i$  of vertex  $i$ , such that  $\prod(k_i) = k_i / \sum_{j \in U_l} k_j$ . Then for each one of the other  $m - n$  edges of the new vertex, choose a community  $U_h (\neq U_l)$  randomly and connect the new vertex to one vertex in  $U_h$  following the preferential attachment mechanism referred above.

The scaling behavior of the degree distribution can be calculated by using several approaches [17, 18, 19]. In our model, the degree distributions  $p(k)$  of vertices of the global network, as well as the local vertices (inside each community), are power-law with exponent 3.0, i.e.,  $p(k) \propto k^{-3.0}$  (see Fig.1). The analytic procedure is simple and not shown here.

As proposed by Newman and Girvan [20] and modified by Kashtan and Alon [21], the strength of community

\*Electronic address: zqfu@ustc.edu.cn

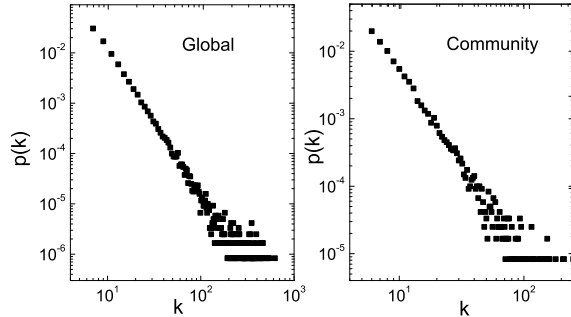


FIG. 1: The global (left) and local (right) degree distribution of the network with  $N = 10^5$ ,  $c = 10$ ,  $m = 4.0$  and  $n = 3.0$ , that says  $Q = 0.65$ . It is worthwhile to point out that, for different values of  $Q$ , the distributions do not change.

structure can be quantified by

$$Q = \sum_1^c \left[ \frac{l_s}{L} - \left( \frac{d_s}{2L} \right)^2 \right], \quad (1)$$

where  $c$  is the number of communities,  $L$  is the number of edges in the network,  $l_s$  is the number of edges between nodes in community  $U_s$ , and  $d_s$  is the sum of the degrees of the nodes in community  $U_s$ . Roughly speaking,  $Q$  is the ratio of the number of edges intra-community to the total number of the edges. Obviously, if the network is divided into some communities more clearly, i.e. there are fewer edges among different communities, the value of  $Q$  is larger. In our model, for large  $N$  (the number of all vertices),  $L = mN$ ,  $l_s = \frac{nN}{c}$  and  $d_s = 2n + (m - n) + (m - n) * (c - 1) / (c - 1) = \frac{2mN}{c}$ . Substituting these results into Eq. (1), we obtain

$$Q = \frac{n}{m} - \frac{1}{c}. \quad (2)$$

Thus, for fixed  $m$  and  $c$ , we modulate the value of  $n$  to get the networks with various community strength  $Q$ .

*III. Epidemic Model.*—We analyze SIRS epidemic model and aim to point out the role of community structure on the temporal dynamics of the epidemic spreading. The disease has three stages: susceptible (S), infected (I), and refractory (R). A vertex of the networked population is described by a single dynamical variable adopting one of these three values. Susceptible elements can pass to the infected state through contagion by an infected one. Infected elements pass to the refractory state after an infection time  $T_I$ . Refractory elements return to the susceptible state after a recovery time  $T_R$ . The contagion is possible only during the S phase, and only by an I element. During the R phase, the elements are immune and do not infect. The system evolves with discrete time steps. Each vertex in the network is characterized by a time counter  $\tau_i(t) = 0, 1, \dots, T_I + T_R \equiv T$ , describing its

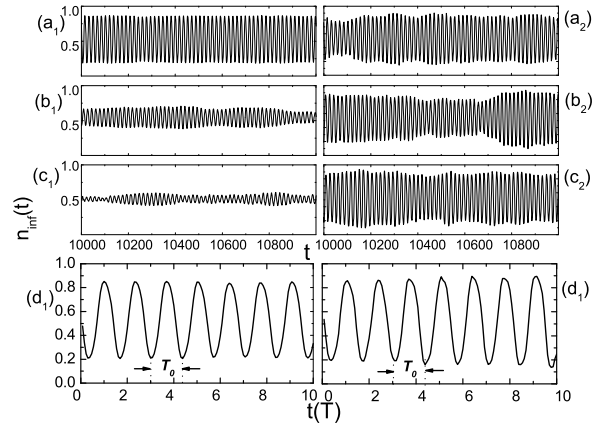


FIG. 2: The time series of the fraction of infected vertices. The systems have  $N = 10^4$ ,  $c = 25$  and  $m = 4.0$ , and the infection cycle with  $T_I = 8$  and  $T_R = 5$ . The left three figures (a1), (b1) and (c1) showed the global fluctuations of  $n_{\text{inf}}(t)$  on the network with  $Q = 0.46, 0.81$  and  $0.935$  respectively. The right three figures showed the local fluctuations correspondingly. It's obvious that the global and local fluctuations are very different. The detailed analysis is presented in the text. The two bottom figures show the clear global (d1) and local (d2) periodic oscillations on the network with weak community structure ( $Q = 0.46$ ). The time steps have been scaled by the natural period  $T$  of the infection cycle.  $T_0$  is the period of the oscillations. It is manifest that  $T_0 > T$ , which is different from the result  $T_0 = T$  presented for SW networks in Ref.[22].

phase in the cycle of the disease. The epidemiological state  $\pi_i$  (S, I, or R) of the vertex depends on the phase in the following way:

$$\begin{aligned} \pi_i(t) &= S & \text{if } \tau_i(t) &= 0 \\ \pi_i(t) &= I & \text{if } \tau_i(t) \in [1, T_I] \\ \pi_i(t) &= R & \text{if } \tau_i(t) \in [T_I + 1, T] \end{aligned} \quad (3)$$

The state of a vertex in the next step depends on its current phase in the cycle, and the state of its neighbors in the network. A susceptible vertex stays as such, at  $\tau = 0$ , until it becomes infected. Once infected, it goes (deterministically) over a cycle that lasts  $T$  time steps. During the first  $T_I$  time steps, it is infected and can potentially transmit the disease to a susceptible neighbor. During the last  $T_R$  time steps of the cycle, it remains in state R, immune and not contagious. After the cycle is complete, it returns to the susceptible state. As mentioned in Ref. [15], if vertex  $i$  is susceptible and it has  $k_i$  neighbors, of which  $k_{\text{inf}}$  are infected, then,  $i$  will become infected with probability  $k_{\text{inf}}/k_i$ .

*IV. Results and Analysis.*—Specifically we study the behavior of the infected sites with respect to  $Q$ . A typical realization starts with the generation of the network characterized by  $Q$  and the initialization of the states of the vertices. The initial fraction of infected vertices

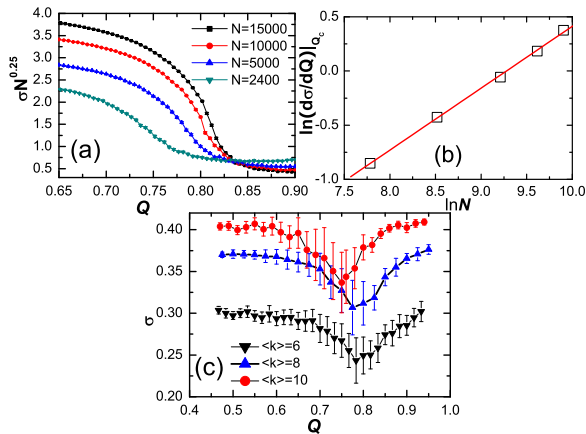


FIG. 3: (Color online) (a) shows the order parameter for global synchronization plotted as  $\sigma N^{\beta/\bar{\nu}}$  with  $\beta/\bar{\nu} = 0.25$  vs  $Q$  for different network size  $N$  with fixed  $Nc = 200$ , where  $Nc$  is the number of vertices in each community. There is given a unique crossing point at  $Q_c = 0.83(5)$ . From (b) we obtained  $(1 - \beta)/\bar{\nu} = 0.57(2)$ . These yield  $\beta \approx 0.30$  and  $\bar{\nu} \approx 1.22$ . (c) displays the order parameter for local synchronization vs  $Q$  for different network mean degree  $\langle k \rangle = 6, 8, 10$  (from bottom to top).

$n_{\text{inf}}(0) = 0.1$  and the rest susceptible, was used in all the simulations here.

After a transient period, a stationary state is achieved. We find that the pronounced fluctuations of the fraction of infected vertices is a function of time. Figure 2 shows three time series displaying the fraction of infected vertices in the network with varying community strength  $Q$ . When  $Q = 0.46$  (see Fig.2(a1)), the network has a weak strength of community structure. It is similar to the real-world networks where the community strength  $Q$  falls in the range from about 0.3 to 0.7 [20]. In such condition, the fraction of infected vertices exhibits large amplitude oscillations. For strong community structure, such as  $Q = 0.81, 0.935$  (see Fig.2(b1) and (c1) respectively), the time series have regular periods but the amplitudes is small and disordered. In addition, we study the local dynamics, that is the epidemic process inside each community. Figure 2(a2), (b2) and (c2) show the time evolution of the fraction of infected vertices in a community, for  $Q = 0.46, 0.81$  and  $0.935$  respectively. The amplitudes are almost the same. Since the amplitude is related to the synchronization of the system, we will give a measure below and make it clearer. Fig. 2(d1) and (d2) show the clear periodic oscillations of the fraction of local and global infected vertices vs the scaled time  $t/T$  while  $Q = 0.46$ , respectively. One can see that the period  $T_0$  is larger than the natural period  $T$  of the infection cycle, which is different from the result on small-world networks presented in Ref. [22]. Moreover, we have done the Fourier power analysis for different  $Q$  and find

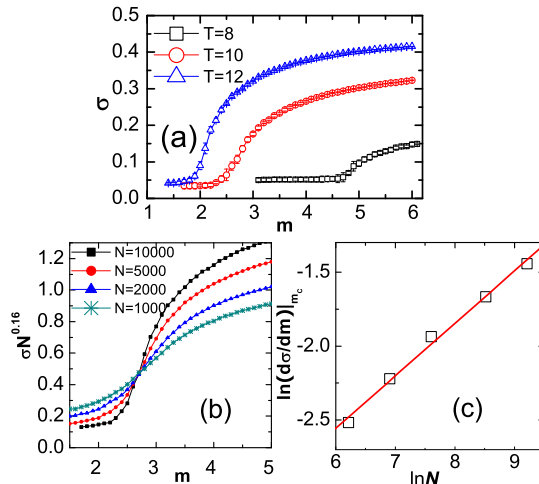


FIG. 4: (Color online) (a) shows the order parameter vs  $m$  for different natural period  $T = 8, 10, 12$ , where  $m = \langle k \rangle / 2$ . (b) displays the order parameter  $\sigma$  for natural period  $T = 10$  plotted as  $\sigma N^{\beta/\bar{\nu}}$  with  $\beta/\bar{\nu} = 0.16$  vs  $m$  for different network size  $N$ . There is given a unique crossing point at  $m_c = 2.80$ . From (c) we obtained  $(1 - \beta)/\bar{\nu} = 0.35(0)$ . These yield  $\beta \approx 0.31$  and  $\bar{\nu} \approx 1.95$ .

that there is a sharp peak in the frequency  $1/T_0$  (not showed here), which reveals that the series have regular temporal periods although the amplitudes are variable. As the difference between  $T_0$  and  $T$  is the time staying at the state S and T is of the same value for all vertices, we could analyze the reason of regular  $T_0$  by estimating the probability  $P_i(t)$  of a vertex  $i$  changing state from S to I at time  $t$ . We here obtain  $p_i(t)$  by using the mean-field estimation as the following,  $p_i(t) = k_{\text{inf}}/k_i \propto n_{\text{inf}}(t)$ . That results implies that all the vertices update their states at almost the same time which induces the regular temporal cycles. Besides the parameter-free infection mechanism, there may be other reasonable choices. For example, if the susceptible had a probability  $\lambda$  of contagion with each infected neighbor, then the probability of infection is  $[1 - (1 - \lambda)^{k_{\text{inf}}}]$ . For small  $\lambda$ , we have  $p_i(t) = [1 - (1 - \lambda)^{k_{\text{inf}}}] \approx \lambda * k_{\text{inf}} \propto n_{\text{inf}}(t)$ . Obviously, that dose not affect the qualitative results here.

To quantify the amplitudes of the oscillation series, we define the relevant order parameter

$$\sigma(t) = \left| \frac{1}{N} \sum_{j=1}^N e^{i\phi_j(t)} \right|, \quad (4)$$

where  $\phi_j = 2\pi(\tau_j - 1)/T$  is a geometrical phase corresponding to  $\tau_j$ . The states  $\tau = 0$  have been left out of the sum in Eq.(4). We obtain the synchronization order parameter  $\sigma$  by averaging over  $10^4$  time steps after the transient to a stationary state and subsequently by aver-

aging over 400 different realizations of the system. Here the synchronization is a measure of the collective order. If at any time  $t$  all the vertices are almost at the same state, i.e.  $\tau_i$  is equal to the same value for all  $i$ , the system is synchronous. While the vertices are at different states equally, the system is not synchronous. Obviously, when the system is not synchronized, the phases are widely spread in the cycle and the complex numbers  $e^{i\phi}$  are correspondingly spread in the unit circle which leads to low value of  $\sigma$ . In contrast, when a significant part of the vertices are synchronized in the cycle,  $\sigma$  is large. The full synchronization, i.e.  $\sigma = 1$ , will be achieved only when all the vertices enter the same state simultaneously. For the local synchronization, we calculate the above order parameter over the vertices in one community.

Precise calculation of the critical community strength  $Q_c$  separating synchronized and desynchronized states requires considering the finite-size effect. In the thermodynamic limit, the order parameter displays the critical behavior  $\sigma \sim (Q - Q_c)^\beta$ , with the critical exponent  $\beta$ . While in a finite system with size much larger than the additional length scale, the critical scaling from is

$$\sigma = N^{-\beta/\bar{\nu}} F[(Q - Q_c)N^{1/\bar{\nu}}], \quad (5)$$

where the exponent  $\nu$  describes the divergence of correlation volume  $\xi_v$  at  $Q_c$ ,  $\xi_v \sim |Q - Q_c|^{-\bar{\nu}}$ . Since at  $Q = Q_c$  the function  $F$  in Eq. (5) has a value independent of  $N$ , plotting  $\sigma N^{\beta/\bar{\nu}}$  vs  $Q$  for various sizes, one can get the value of  $\beta/\bar{\nu}$  that gives a unique crossing point at  $Q_c$ . One then use

$$\ln\left[\frac{d\sigma}{dQ}\right]_{Q_c} = \frac{1-\beta}{\bar{\nu}} \ln N + const \quad (6)$$

in order to determine the value of  $(1-\beta)/\bar{\nu}$ . Then the exponent  $\beta$  and  $\bar{\nu}$  can be figured out. Figure 3(a) displays the determination of  $Q_c$  for the global synchronization using the finite-scale form Eq. (5). Varying the value of  $\beta/\bar{\nu}$  we find that  $\beta/\bar{\nu} \simeq 0.25$  gives a well-defined crossing point at  $Q_c \simeq 0.835$ . In Fig. 3(b), the least-square fit to Eq. (6) gives  $(1-\beta)/\bar{\nu} \simeq 0.572$ . These yield  $\beta \approx 0.30$  and  $\bar{\nu} \approx 1.22$ . Moreover, as showed in Fig. 3(c), for different mean degree  $\langle k \rangle$ , the local synchronization parameter falls into the pit around a value  $Q \approx 0.75$ . This implicates that, when the communities are almost unattached (i.e. for very large  $Q$ ) the local dynamic lies on the inner structure of community independently, while the communities couple each other strongly (for small  $Q$ ),

the local dynamic is almost the same as the global one, and in the midst the local synchronization is the weakest.

Further more, we have studied the impact of the mean degree  $\langle k \rangle$  of scale-free networks upon the synchronization. We start the simulation with a generation of scale-free networks with  $Q = 0$ , that is the BA model or our model with  $n/m = 1/c$ , and the initial fraction of infected vertices  $n_{\text{inf}}(0) = 0.1$ . We let the number of vertices  $m$  that a new added vertex will connect be real number, as referred in *section II*. Obviously,  $\langle k \rangle = 2m$ . Fig. 4(a) shows the order parameter  $\sigma$  vs  $m$  for different period  $T$  of the infection cycle. For a fixed period  $T$ , a transition in the synchronization can be observed as  $m$  increases. Moreover, the larger the period  $T$ , the less the critical value of  $mc$ , at which the transition occurs. We set  $T = 10$  to analyze the critical scaling by using standard finite-size analysis mentioned above. Fig. 4(b) displays that when  $\beta/\bar{\nu} = 0.16$  the curves with different sizes  $N$  give a unique crossing point at  $m_c \approx 2.8$  (where  $\langle k \rangle_c \approx 5.6$ ). In Fig. 4(c), the fit gives  $(1-\beta)/\bar{\nu} \simeq 0.35$ . Hence  $\beta \simeq 0.31$  and  $\nu \simeq 1.95$ .

*V. Conclusion.*—To summarize, we have investigated the influence of the strength of community structure ( $Q$ ) on global and local synchronization induced by the SIRS epidemic dynamics. The numerical results have shown that small  $Q$  induces better global synchronization and a phase transition occurs at  $Q_c \approx 0.835$  estimated by using finite size analysis; While for the local synchronization there exists a minimal value of order parameter  $\sigma$  around  $Q \approx 0.75$ . This result is in accordance with Ref. [23] in which a modified simulated annealing algorithm is applied to optimize the synchronizability and well-defined communities do not exit in the emerging networks. That implies the networks with small  $Q$  are of strong synchronizability. It is also worth mentioning that, as in synchronization process well-defined communities of nodes emerge in different time scales, Arenas *et al* have used the synchronization to reveal the community structure [24].

Moreover, we have studied the synchronization order parameter vs  $\langle k \rangle$  on scale-free networks with  $Q = 0$ . The simulation results demonstrate that, for a fixed period  $T$ , a transition in the synchronization can be observed as  $\langle k \rangle$  increases. The larger period  $T$  corresponds to smaller critical value of transition point  $\langle k \rangle_c$ .

We acknowledge the support from the National Natural Science Foundation of China under Grants No. 71471033 and No. 70671097.

---

[1] R. Albert and A. -L. Barabasi, *Rev. Mod. Phys.* **74**, 1 (2002).  
 [2] S. N. Dorogovtsev and J. F. F. Mendes, *Adv. Phys.* **51**, 1079 (2002).  
 [3] M. E. J. Newman, *SIAM Rev.* **45**, 167 (2003).  
 [4] R. Pastor-Satorras and A. Vespignani, *Evolution and*

*structure of the Internet: a statistical physics approach* (Cambridge University Press, 2004).

[5] R. Pastor-Satorras and A. Vespignani, *Phys. Rev. Lett.* **86**, 3200 (2001).  
 [6] M. Barthélemy, A. Barrat, R. Pastor-Satorras, and A. Vespignani, *Phys. Rev. Lett.* **92**, 178701 (2004).

- [7] T. Nishikawa, A. E. Motter, Y.-C. Lai and F. C. Hoppensteadt, *Phys. Rev. Lett.* **91**, 014101 (2003).
- [8] V. M. Eguíluz and K. Klemm, *Phys. Rev. Lett.* **89**, 108701 (2002); M. Boguñá, R. Pastor-Satorras, and A. Vespignani, *Phys. Rev. Lett.* **90**, 204101 (2003).
- [9] M. Timme, F. W. and T. Geisel, M. Chavez, D.-U. Hwang, A. Amann, H. G. E. Hentschel and S. Boccaletti, *Phys. Rev. Lett.* **94**, 218701 (2005).
- [10] D.-H. Kim, B. J. Kim and H. Jeong, *Phys. Rev. Lett.* **94**, 025501 (2005).
- [11] M. E. J. Newman, *Phys. Rev. E* **64**, 016131 (2001); M. Girvan and M. E. J. Newman, *Proc. Natl Acad. Sci. USA* **99**, 7821 (2002).
- [12] G. Palla, I. Derényi, I. Farkas and T. Vicsek, *Nature* **435**, 814 (2005).
- [13] N. Bailey, *Epidemic Theory of Infectious Diseases and its Applications* (Hafner Press, 2004).
- [14] R. M. Anderson and R. M. May (ed.), *Population Biology of Infectious Diseases* (Springer, Berlin, 1982).
- [15] M. Kuperman and G. Abramson, *Phys. rev. Lett.* **86**, 2909 (2001).
- [16] A.-L. Barabási and R. Albert, *Science* **286**, 509 (1999).
- [17] A.-L. Barabási, R. Albert and H. Jeong, *Physica A* **272**, 173 (1999).
- [18] S. N. Dorogovtsev, J. F. F. Mendes and A. N. Samukhin, *Phys. Rev. Lett.* **85**, 4633 (2000).
- [19] P. L. Krapivsky, S. Redner and F. Leyvraz, *Phys. Rev. Lett.* **85**, 4629 (2000).
- [20] M. E. J. Newman and M. Girvan, *Phys. Rev. E* **69**, 026113 (2004).
- [21] N. Kashtan and U. Alon, *Proc. Natl Acad. Sci. USA* **102**, 13773 (2005).
- [22] P. M. Gade and S. Sinha, *Phys. Rev. E*, **72**, 052903 (2005).
- [23] L. Donetti, P. I. Hurtado and M. A. Muñoz, *Phys. Rev. Lett.* **95**, 188701 (2005).
- [24] A. Arenas, A. Díaz-Guilera and C. J. Pérez-Vicente, *Phys. Rev. Lett.* **96**, 114102 (2006).